Efficiency Improvement of a High-Speed Permanent Magnet Excited Synchronous Machine by the use of Spot-Welding as Lamination Packaging Technology

David Ukwungwu, Nora Leuning and Kay Hameyer
Institute of Electrical Machines (IEM), RWTH Aachen University

***Abstract*—In this paper, an efficiency improvement of a high-speed permanent magnet excited synchronous machine (PMSM) by the use of spot-welding as lamination packaging technology is realized. Welding, interlocking, clinching and gluing are typical technologies to manufacture electrical steel stacks of electrical machines. However, these processes deteriorate the magnetic properties of the steel sheets, thereby decreasing the overall efficiency of the machine. Variations of line-welding (six, eight, twelve, thirty two and forty) line welds and spot-welding procedure is performed and analyzed. A semi-physical iron loss separation approach is used to extract the IEM iron loss model [6]. These parameters are utilized during the finite element simulation to calculate the effective iron loss (efficiency) of the machine while using each joining procedure. A low speed, high-speed and WLTC-c3 driving cycle is exemplarily used to analyze the effects of each procedure on the machine efficiency at the different operating conditions.**

***Index Terms*—welding process, ferro-magnetic lamination, numerical simulation, electrical steel**

I. Introduction

For the construction of a mechanically stable magnetic core of an electrical ac machine, the electrical steel laminations must be firmly connected. Welding, interlocking, clinching and gluing represent the current state of the art of the mechanical connection of such thin steel sheets. Each of the connecting processes leads directly to the deterioration of the material's magnetic properties. Increased iron losses as well as a decreasing permeability of the electrical steel can be observed. The connection of the single lamination sheets by welding is a commonly used technology. In this process, the sheets are joined mechanically along a seam accompanied by an apparent dissipation of heat along the welding area. This local concentration of dissipated heat yields a thermal degradation and increase of the residual stress distribution inside the material. The residual stress reduces the magnetizability of the electrical steel used due to the Villari-effect. In this paper, a method for improving the overall efficiency of a high-speed permanent magnet synchronous machine is discussed. The decreasing effects of the aforementioned weld process (spot-welding) on the eddy-current loss component of iron loss can be utilized for a high-speed operation, where most of the operations are at higher frequencies in the range $400\,\mathrm{Hz}$ - $1000\,\mathrm{Hz}$. A finite element simulation of the high-speed permanent magnet synchronous machine is performed and the analysis of the joining process with driving cycles has been done. The effects of welding have been reported [1]–[3] to lead to a significant magnetic deterioration of the sample of a ring core. These deterioration are in part, due to increase of the average grain size in and around the welded area, and also due to the increase in residue stresses in and around the weld-point [5], [8], [10], [12]. However, a comprehensive and systematic analysis of the welding process is still lacking. This paper studies the effects of different welding scheme such as spot-welding and line-welding on the iron losses and efficiencies of electrical machines. The simulated results will then be evaluated with vehicle data and driving cycles with view of understanding the exact extent of the influence of welding on actual application.

II. Experimental Approach

A. Examined samples

Ring core samples welded with spot-welding and line-welding procedure were manufactured for this study. The ring core laminations have inner D_i and outer D_o diameters of $60\,\mathrm{mm}$ and $48\,\mathrm{mm}$ respectively (Fig. 1).

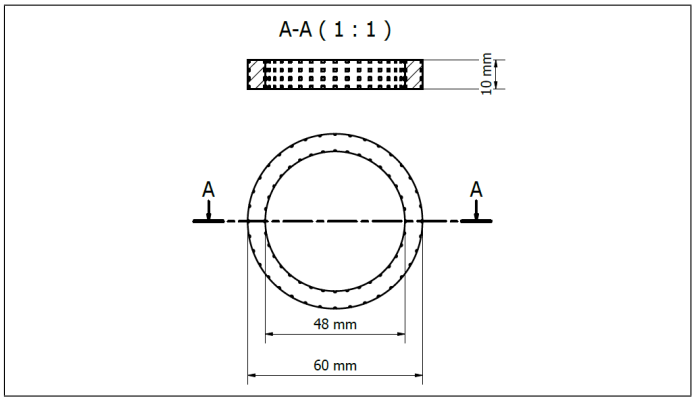

Figure 1: Geometry of the samples.

The height h of the examined ring samples is $9\,\mathrm{mm}$, i.e. 30 ring laminations are joined together. The reference ring core is joined together with a conventional glue, so as to exclude the effects of the material degradation. The specific iron loss and magnetization emanating from this sample represents the electromagnetic properties of the laminated stack. The individual rings are laser cut to the aforementioned dimensions.

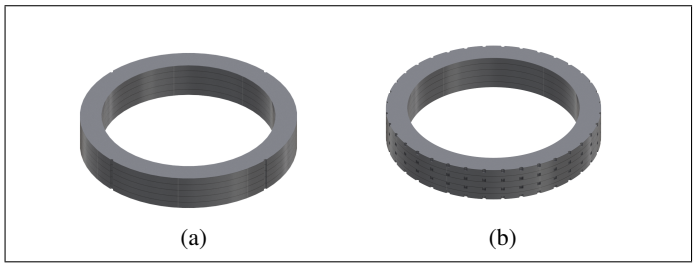

(a) (b)

Figure 2: (a) Line-weld sample and (b) Spot-weld sample.

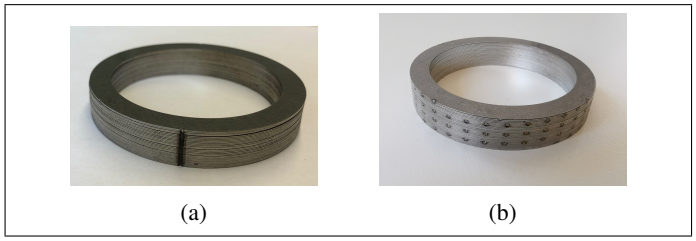

(a) (b)

Figure 3: (a) Line-weld sample and (b) Spot-weld sample.

The reference ring core is compared to other ring cores of different welding concepts (spot- and line-welding). The spot welded ring cores connects only two to three rings per spot at each instance 3b). There is a minimum of 4 welds on each rings to ensure the mechanical stability of the motor. Less spot-welds can be used depending the mechanical requirements of the application.

Table I: Specification of the used laser beam source.

Producer	TRUMPF
Model	TruDisc 16002
Medium	Yb:YAG
Type	Disc-Laser Multi-Mode
Power range [W]	320–16000
Wavelenght λ [nm]	1030
Fibre diameter [µm]	200

For the welding process, a laser beam power of $320\,\mathrm{W}$, focal position of $0\,\mathrm{mm}$, resulting in a focal diameter of $400\,\mu\mathrm{m}$ and working pressure of $1000\,\mathrm{mbar}$. Whereas the line-welds are performed at a weld speed of $0.5\,\mathrm{m/min}$, the spot welds are instantaneous at a pulse duration of $70\,\mathrm{ms}$. To ensure the comparability of the ring cores, all other weld process parameters are held constant. A multi-mode disc-laser with a focal length of $400\,\mathrm{mm}$ is used for this study (Tab. I). Both spot- and line welding are performed with the laser.

B. Measurement method

In the measurement setup, during the sample preparations, the ring core dimensions (magnetic length, effective active area and effective active volume) are calculated according to DIN-IEC-60205 standard. During measurement the current on the primary winding induces a voltage response on the secondary winding. With the voltage response the magnetic parameters are derived according to DIN-IEC-60404-6 standard.

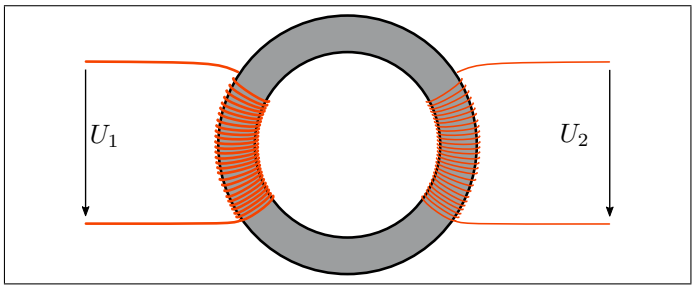

Figure 4: Measurement setup.

$$H = \frac{N_1 \cdot I}{l_m} \tag{1}$$

The magnetic field strength H is calculated from the current I on the primary winding and magnetic length l_m see equation 1.

$$\overline{U_2} = 4 \cdot f \cdot A \cdot B \cdot N_2 \tag{2}$$

$$P_s = \frac{N_1 \cdot P_m}{m \cdot N_2} - \frac{\pi \cdot (\overline{U_2})^2}{2 \cdot \sqrt{2} \cdot m \cdot R_i} \tag{3}$$

The specific iron loss P_s is then derived from the induced voltage on the secondary winding and the ring core geometry (area) see equation 3 . Whereas P_m and m are the measured iron loss and ring core weight respectively. The ring cores are wound with 80 turns on the primary N_1 and secondary side N_2.

III. Measurement Results

In this section, the extent to which each welding scheme contributes on the magnetic deterioration of the electrical sheets is quantified and analyzed. In Fig. 5 and 6 the measured results of the specific iron loss and magnetization curves at $50\,\mathrm{Hz}$ is shown.

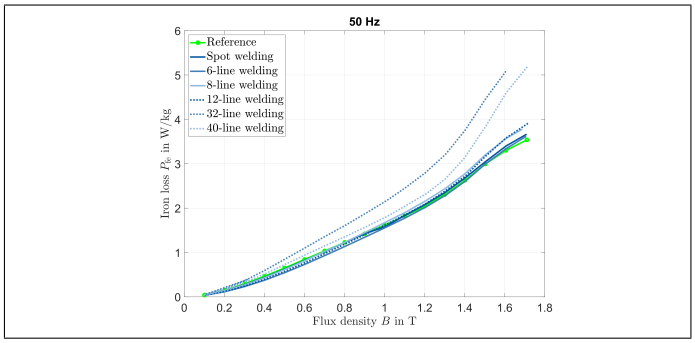

Figure 5: Specific iron loss at $50\,\mathrm{Hz}$.

it can be observed, that in general welding leads to the degradation of the electromagnetic properties of the material. This is due to an apparent increase in the thermal energy that penetrates into the sheets. This energy leads to the change of the effective grain size and the deposition of residual stress at the affected area [4], thereby leading to the magnetic deterioration of the sheets. The level of deterioration increases

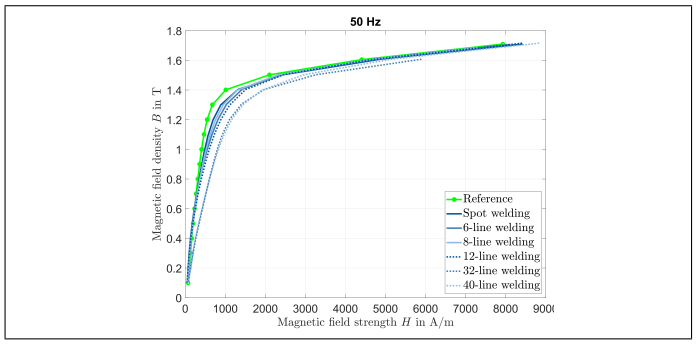

Figure 6: Magnetization curve at 50 Hz.

with increasing number of weld lines. The spot welded sample is compared to the 8-line welded sample because of a similar effective welded area of $12.44\,\mathrm{mm}^2$. It is observed that the decrease of the magnetization of the welded samples, when compared to the reference sample is more pronounced at flux densities between 0.6 T and 1.5 T. At high frequencies, Fig. 7 and 8 depicts a more significant deterioration of the material magnetic properties compared to the reference sample. This is due to the effects of the increasing grain sizes, which increases the excess and non-linear loss component.

The non-dependency of the eddy-current loss from the effects

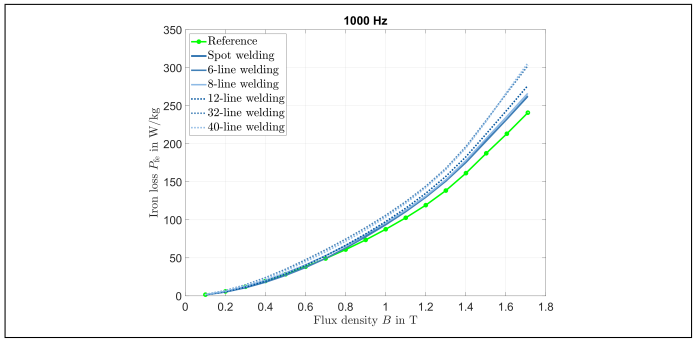

Figure 7: Specific iron loss at1000 Hz.

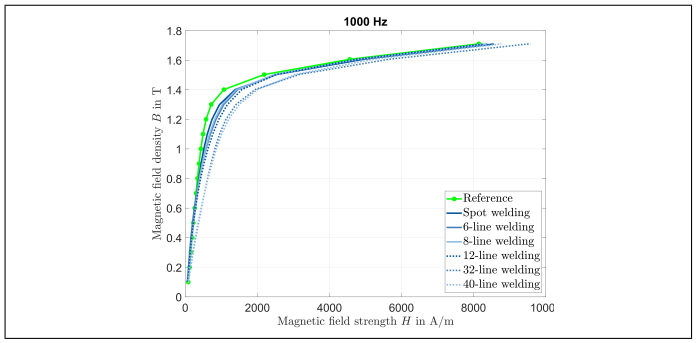

Figure 8: Magnetization curve at1000 Hz.

of welding is observed, at the relatively slight percentage of deterioration of the material for both low and high frequencies. The difference in the deterioration of iron losses at higher frequencies compared to lower frequencies can be attributed to the grain size dependency of the excess loss component of iron loss. Furthermore, there was a slight change of the magnetization curves with increasing frequencies Fig. 6 and 8 observed. Therefore, the effects of welding on the magnetization of the ring core is also frequency dependent. In Fig. 9 and 10 is the depiction of deterioration of the iron loss of the investigated ring samples at a flux density of 1 T and frequencies of 50 Hz and 1000 Hz respectively. It can be observed, that line-welding leads to more deterioration compared to spot-welding. It can also be observed, that spot-welding and line-welding with 4 lines performed better than the reference sample. This effect will be evaluated in details, because it could be from the margin of error or due to changes in grain texture around the weld-point. The Fig.

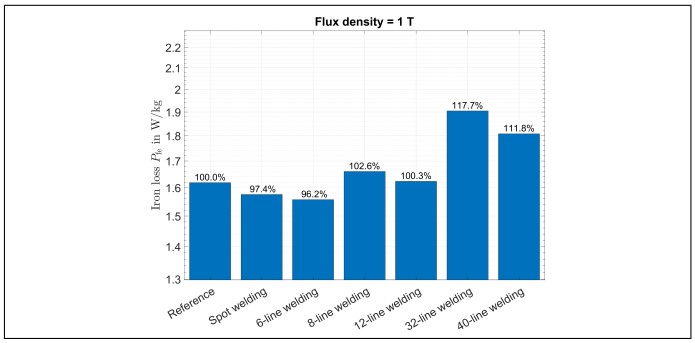

Figure 9: Specific iron loss changes at1 T and 50 Hz.

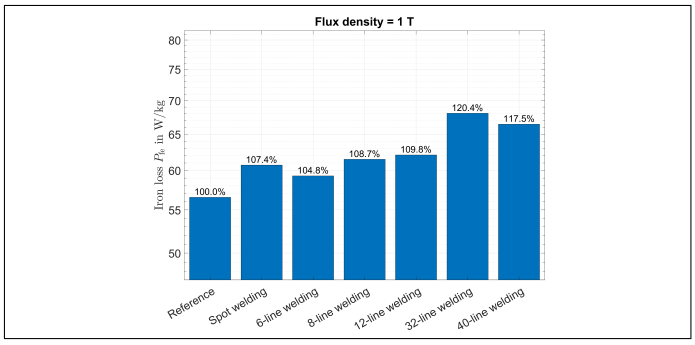

Figure 10: Specific iron loss changes at 1 T and 1000 Hz.

11 and 12 depicts the magnetization value of the investigated ring samples at a flux density of 1 T and frequencies of 50 Hz and 1000 Hz respectively. It can be seen, that the deterioration tendency is independent on the frequency. A higher level of deterioration of magnetization is observed compared to degradation of the iron loss. The total iron loss is defined as the sum of the hysteresis loss, classic eddy-current loss, local eddy-current loss component (excess) and non-linear loss component [6].

$$P_{total} = a_1 \cdot B^{\alpha} \cdot f + F_{skin} \cdot a_2 \cdot B^2 \cdot f^2 \cdot (1 + a_3 \cdot B^{a_4}) + a_5 \cdot B^{1.5} \cdot f^{1.5} \quad (4)$$

Whereby a_1, α are the hysteresis loss parameter and the exponential coefficient of the hysteresis loss, a_2, a_5 are classical eddy-current loss constant and excess loss constant respectively and a_3, a_4 are the non-linear loss constants [6]. As can be seen in equation 4, the excess loss component is

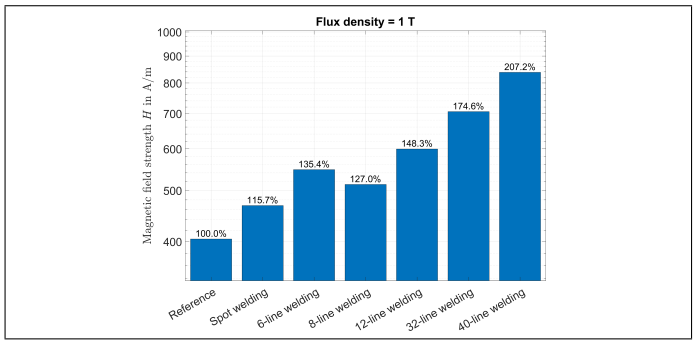

Figure 11: Magnetization changes at 1 T and 50 Hz.

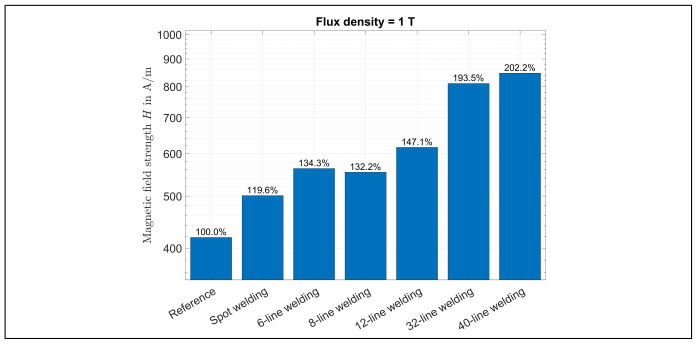

Figure 12: Magnetization changes at 1 T and 1000 Hz.

proportional to the frequency to power 1.5. This meant that an increase in excess loss component gets more pronounce at higher frequencies leading to more specific iron loss generation.

IV. FEM SIMULATION

For the proposed FEM-simulation comes the motor topology. A high speed permanent magnet synchronous motor PMSM with four poles, an axial length of 98 mm and three-phased winding. The Fig. 13 depicts the torque-speed map of the attainable efficiency, when the material is welded with the line-welding scheme. In table II is the data of the simulated machine shown.

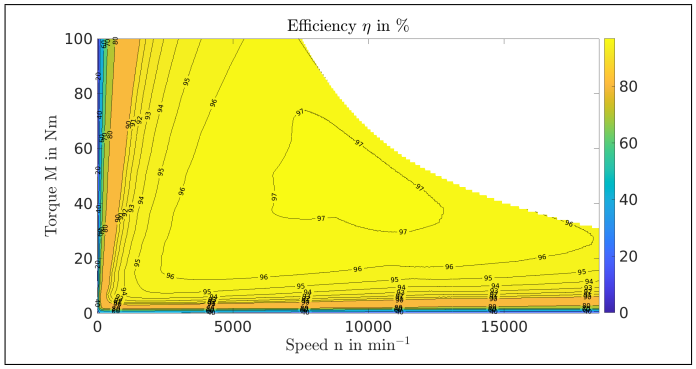

Figure 13: Torque-speed map of the efficiency.

Table II: Data of the simulated machine.

Machine parameter	Units	Values
maximum torque	Nm	100
maximum speed	min^{-1}	18000
rated voltage	V	300
no of slots	–	36
outer diameter	mm	200
axial length	mm	98

V. EVALUATION OF THE RESULT

After modeling of the vehicle (here: Volkswagen golf), the operating points of the different driving cycles are calculated from the velocity-time characteristics of each driving cycle. The motor is incorporated so as to evaluate the motor characteristics with respect to the efficiencies and losses at the different operating points. An algorithm is used to calculate the operating points (torque and rotational speed) values equivalent of the driving cycles at an allowed maximum vehicle velocity of 180 km/h. Fig. 14, 15 and 16

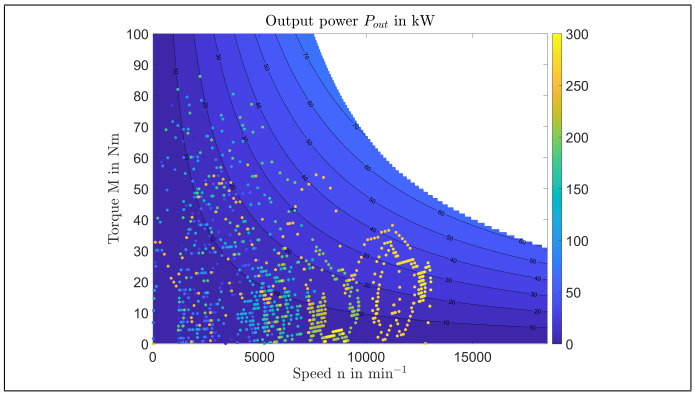

Figure 14: Torque-speed map of the WLTC-c3 driving cycle.

show the depiction of the operating points emanating from WLTC-c3, city and highway driving cycles respectively. These points show exactly the torque-speed characteristics of the respective driving cycle. After the calculation of the torque

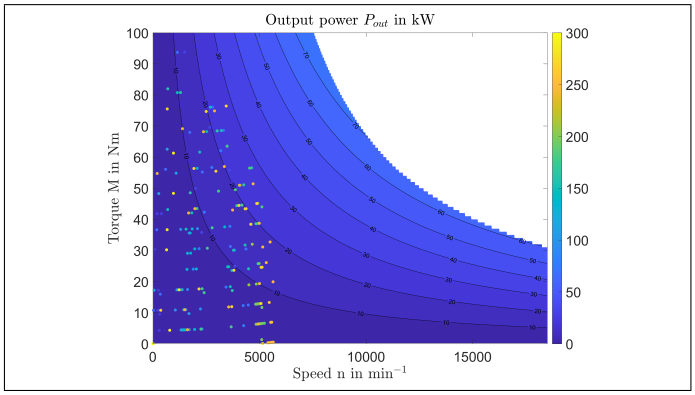

Figure 15: Torque-speed map of the city driving cycle.

and rotational speed equivalent of the driving cycles, i.e. operational points and its distributions (Prob(M_{cycle},n_{cycle},α)) are then incorporated into the loss map of the motor. Whereas

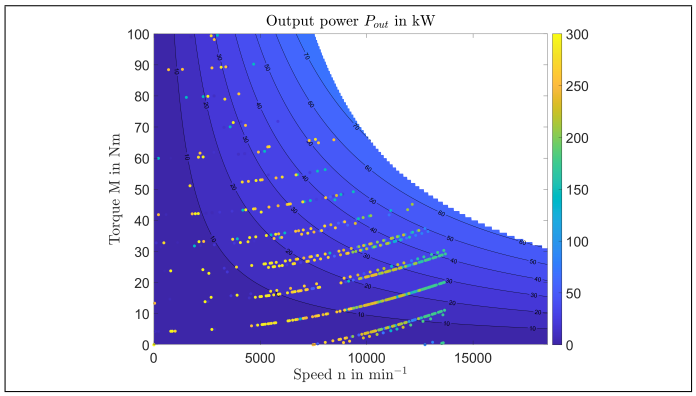

Figure 16: Torque-speed map of the highway driving cycle.

α represents here the utilized driving cycle. The mathematical description of the aforementioned process can be seen in equation 5.

$$P(M_{cycle}, n_{cycle}, \alpha, \beta) = P(M_{motor}, n_{motor}, \beta) \cdot Prob(M_{cycle}, n_{cycle}, \alpha) \quad (5)$$

Where $P(M_{motor}, n_{motor}, \beta)$ are the motor loss power depending on the used welding scheme β. Afterwards the corresponding losses at various operating points were then calculated by the integration of equation.

$$P(\alpha, \beta) = \int \int P(M_{cycle}, n_{cycle}, \alpha, \beta)\ dM_{cycle}\ dn_{cycle} \quad (6)$$

Due to the fact that loss energy and not loss itself is the most appropriate value for the evaluation of a drive's efficiency during a traction's operation, the total loss energies of the corresponding driving cycles were calculated. The calculation were done according to equation 7.

$$E(\alpha, \beta)\ [kWh] = P(\alpha, \beta)\ [kW] \cdot \frac{total\ time}{3600s} \quad (7)$$

The calculated loss energy in equation 7 of each driving cycle

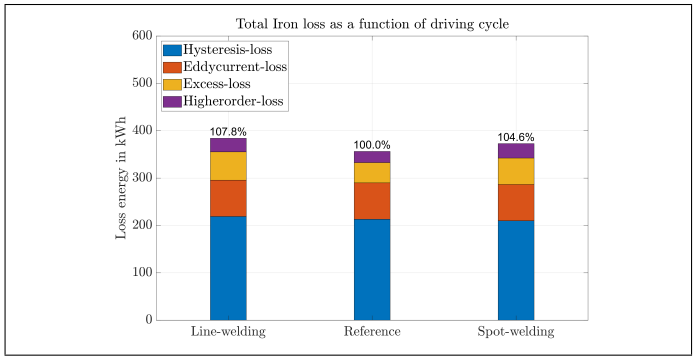

Figure 17: Iron loss while operating the WLTC-c3 driving cycle.

is then depicted against the different packaging technology. The Fig. 17, 18 and 19 depict these losses depending on the WLTC-c3, city and highway driving cycles. It can be seen in all driving cycle, that there is no observable influence of welding on the eddy current loss component of iron loss. High observable change in the excess loss component of iron loss, due to the its high negative dependency on the average grain size. Welding processes leads to an increase of the average grain size at the welded area, because of the influx of thermal energy into the material. The welding parameters such as laser power or welding speed influence the rate of diffusion of the thermal energy into the steel sheet. The rate of diffusion during spot-welding is slower, due to the higher welding speed (spontaneous) associated with the welding scheme. This meant, that the increase in grain sizes is relatively smaller during spot-welding as with line-welding. Fig. 17 shows the iron loss energy dissipated during the

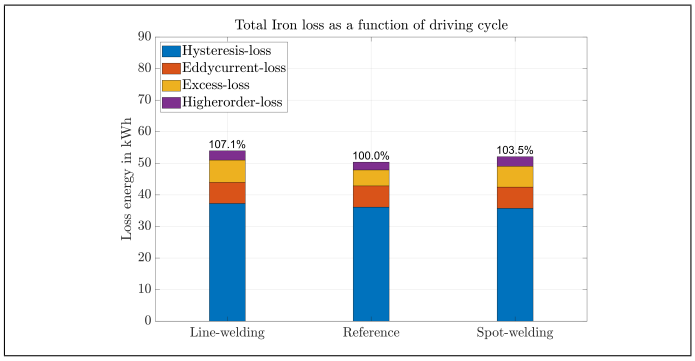

Figure 18: Iron loss while operating the city driving cycle.

WLTC-c3 driving cycle. It can be seen, that whereas $4.5\,\%$ more loss energy is dissipated with spot-welding compared to the reference, $7.8\,\%$ more loss energy can be attributed to the line-welding scheme. A total reduction of $3.3\,\%$ loss energy can be attained by the use of spot-welding as lamination packaging method instead of the conventional line-welding scheme. Fig. 18 depicts the iron loss energy dissipated during the city driving scheme. It can be observed, that the value of excess loss energy is higher than the eddy current loss energy during the city driving scheme with line-welding, this is due to the low or average speeds attributed to this driving cycle, at which the influence of excess loss component of iron loss becomes more pronounced. This is the reason for an increased reduction of the total dissipated loss energy of around $3.6\,\%$. A less rate of diffusion leads to the performance improvement of the drive train during the city driving scheme. Fig. 19 shows in average more deterioration of the electromagnetic properties of the electrical steel sheet. This is in part due to the probability of higher rotational speeds and also to the magnetization of the utilized electrical steel sheet. The higher value of the hysteresis loss energy attributed to line-welding as spot-welding is apparently due to the effects of the residue stresses accompanied with welding. Due to higher frequencies, there is less improvement compared to other driving cycles.

VI. Conclusions

To analyze the effects of different welding schemes on the loss dissipation (efficiency) of an electric drive train, the

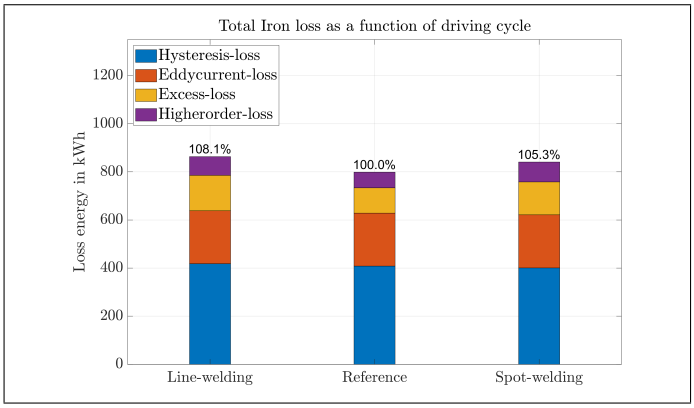

Figure 19: Ironloss while operating the highway driving cycle.

ring core samples were electromagnetically measured. Loss dissipation attributed to a reference sample (ring packaged with a conventional glue), a spot welded and conventional line welded sample are compared and analyzed. A more visible deterioration of the magnetization was observed for all welded ring cores at flux densities between $0.6\,\mathrm{T}$–$1.5\,\mathrm{T}$ and at all frequencies during the electromagnetic measurements. For the evaluation of the results, a model incorporating the machine data with the application (golf-vehicle) and driving cycle characteristics is utilized. This modeling approach helps in mapping out of the knowledge on component level to system-wide investigations. Little or no influence of welding on the dissipated eddy current loss energy is observed, because the connection of only the outer surface has an insignificant influence on the induced eddy current. A higher performance improvement of the drive train was achieved at low and average speeds, due to the effects of average grain size at the welded area. Reduction of the excess loss component leads to a higher level of improvement due to its dependency on the grain size of the electrical steel grade. It can be seen, that a reduction of the hysteresis loss component with spot-welding in comparison with line-welding was due to the effects of residue stresses associated with welding. The improvement of the overall efficiency of the motor through spot-welding is due its lower iron loss compared to line-welding. The use of spot-welding procedure leads to less degradation compared to conventional line-welding procedure. This research shows, that a system-wide improvement of the motor can be achieved with welding procedural change (spot-welding) instead of line welding.

Acknowledgment

The work is funded by the Deutsche Forschungsgemeinschaft (DFG) 432930813 in the research group project “Elektromagnetische Bewertung und Quantifizierung von Schweißprozessen zur Paketierung von Elektroblechen”. Simulations were performed with computing resources granted by RWTH Aachen University under project rwth0922.

References

[1] W. M. Arshad, T. Ryckebush, F. Magnussen, H. Lendenmann, J. Soulard, B. Eriksson, and B. Malmros,“Incorporating Lamination Processing and Component Manufacturing in Electrical Machine Design Tools” in Conference Record of the 2007 IEEE Industry Applications Conference, 2007. 42nd IAS Annual Meeting, 2007, pp. 94–102.

[2] A. Krings, S. Nategh, O. Wallmark, and J. Soulard, “Influence of the Welding Process on the Performance of Slotless PM Motors With SiFe and NiFe Stator Laminations,” IEEE Transactions on Industry Applications, vol. 50, no. 1, pp. 296–306, Jan. 2014.

[3] A. Schoppa, J. Schneider and C.-D. Wuppermann, “Influence of the manufacturing process on the magnetic properties of non-oriented electrical steels”, Journal of Magnetism and Magnetic Materials 215-226 (2000) 74-78.

[4] Krichel, T., S. Olschok und U. Reisgen (2021): Laser in Vacuum spot welding of electrical steel sheets with 3.7 % Si-content. In: LiM - Lasers in Manufacturing Conference, June 21 - 24, 2021.

[5] N. Leuning, S. Steentjes, B. Gerhards, U. Reisgen, Kay Hameyer, “Analysis of a novel laser welding strategy for electrical steel laminations”, 7th International Electric Drives Production Conference EDPC 2017, Nürnberg, Germany.

[6] D. Eggers, S. Steentjes, and K. Hameyer. ”Advanced iron-loss estimation for nonlinear material behavior.” IEEE Transactions on Magnetics 48.11 (2012): 3021-3024.

[7] G. Bertotti, “General properties of power losses in soft ferromagnetic materials,” IEEE Transactions on Magnetics, vol. 24, no. 1, pp. 621–630, Jan. 1988.

[8] E. Lamprecht, M. Hömme, and T. Albrecht, “Investigations of eddy current losses in laminated cores due to the impact of various stacking processes,” in Electric Drives Production Conference (EDPC), 2012 2nd International, 2012, pp. 1–8.

[9] S. Imamori, S. Steentjes, K. Hameyer, “Influence of interlocking on magnetic properties of electrical steel lamination”, IEEE Trans. Mag., Volume 53, Nr. 11, 2017, pp 1-4.

[10] N. Leuning, S. Steentjes, K. Hameyer, „Effect of grain size and magnetic texture on iron-loss components in NO electrical steel at different frequencies“, Journal of Magnetism and Magnetic Materials, Bd. 469, S. 373–382, 2019.

[11] N. Leuning, S. Steentjes, H. A. Weiss, W. Volk, K. Hameyer, „Magnetic Material Deterioration of Non-Oriented Electrical Steels as a Result of Plastic Deformation Considering Residual Stress Distribution“, IEEE Trans. Mag., Bd. 54, Nr. 11, S. 1–5, 2018.

[12] L. Luming, H. Songling, W. Xiaofeng, S. Keren, and W. Su, “Magnetic field abnormality caused by welding residual stress,” Journal of Magnetism and Magnetic Materials, vol. 261, no. 3, pp. 385–391, May 2003.

[13] F. Pfeifer and W. Kunz, “Bedeutung von Kornstruktur und Fremdkörpereinschlüssen für die Magne-tisierungseigenschaften hochpermeabler Ni-Fe-legierungen,” Journal of Magnetism and Magnetic Materials, vol. 4, no. 1–4, pp. 214–219, Jan. 1977.

[14] T. Schade, R. M. Ramsayer, and J. P. Bergmann, “Laser welding of electrical steel stacks investigation of the weldability,” in Electric Drives Production Conference (EDPC), 2014 4th International, 2014, pp. 1–6.

[15] Schade, T. e. a. (2014): Electrical steel stacks for traction motors - fundamental investigation of the weldability. In: Shaping the Future by Engineering: Proceedings; 58th IWK, Ilmenau Scientific Colloquium, Vol. 58.

[16] D. Schmidt, M. van der Giet, and K. Hameyer, “Improved iron-loss prediction by a modified loss-equation using reduced parameter identification range”, 20th Int. Conf. on Soft Magnetic Materials (SMM20), p. 421, Kos, Greece, 2011.

[17] N. Leuning, S. Steentjes, K. Hameyer, „Effect of magnetic anisotropy on Villari Effect in non-oriented FeSi electrical steel”, International Journal of Applied Electromagnetics and Mechanics, Bd. 55, Nr. S1, S. 23–31, 2017.

[18] H. Wang, Y. Zhang, S. Li, „Laser welding of laminated electrical steels”, Journal of Materials Processing Technology, 230, 99-108, (2016).

[19] D. Ukwungwu, T. Krichel, B. Schauerte, N. Leuning, S. Olschok, U. Reisgen, K. Hameyer, ”Electromagnetic assessment of welding processes for packaging of electrical sheets”, 2020 10th International Electric Drives Production Conference (EDPC), 2020, pp. 1-6.